Progress In Electromagnetics Research C, Vol. 119, 125–134, 2022

Dual Band Two Element Rim Based MIMO Antennas with Coupling Manipulation for Low SAR Mobile Handsets

Muhammad A. Jamshed[1, *], Tim W. C. Brown[2], and Fabien Héliot[2]

Abstract—In this paper, the mutual coupling from a multiple-input-multiple-output (MIMO) rim antenna has been utilized to control the level of specific absorption rate (SAR), when the mobile handset comes in close contact to the human body. The proposed antenna is capable of operating at 2.1 GHz and 4.3 GHz, respectively. A periodic defective ground structure (DGS) in conjunction with diodes and capacitors are used to manipulate the coupling between antenna elements. The working of the proposed dual band antenna design is validated using the characteristic mode analysis (CMA), and the current distribution. The MIMO performance is studied by using envelope correlation coefficient (ECC) and loss in capacity analysis. The effect of hand and LCD on the antenna performance is shown. The SAR analysis shows up to 30% reduction, in comparison to the baseline value of the SAR of the proposed antenna design.

1. INTRODUCTION

The multiple input multiple output (MIMO) technology is considered as a decisive technology to enhance the channel capacity and spectrum efficiency for the future wireless communication systems [1]. The main way to increase the capacity at the user terminal (UT) is by increasing the number of active antenna elements, but their number is restricted by the space limitation at the UT [2]. A plethora of research efforts have been put up to increase the number of active elements without degrading the MIMO performance. For instance, in [2], 8-element MIMO antenna array for metal-rimmed 5G-enabled smartphone is proposed by using a composite structure of slot and loop antenna. In [3], a wide-band metal rimed 8×8 MIMO antenna is proposed for 5G smartphones, which integrates the dual antenna pair and orthogonal modes to achieve the desired isolation and the envelope cross co-relation (ECC). Although, all of these research efforts and many others just focus on using different techniques, i.e., neutralization lines [4, 5], etc. to increase the number of active antenna elements, while still meeting the MIMO performance, yet none of them have focused on the variation in electromagnetic field (EMF) coupled to the human head, which is quantified by the specific absorption rate (SAR) [6].

There are numerous ways that can be employed to reduce SAR, i.e., through ferrites [7, 8], metamaterials [9], etc. but the space limitation at the UT and the complexity of these design makes it nearly impossible to keep the SAR within the set limits. However, the existing work on designing of the antennas for UT does not aim at controlling/reducing the SAR during the usage and just only show that the SAR adhere to safety limits. The low SAR values reported in [10, 11] are actually due to the alignment of the single rim antenna element away from the ear (see Fig. 20 in [10] and Fig. 7(c) in [11]), and does not consider the MIMO configuration during the SAR calculation. Similarly, in [12] the authors do not show any results related to the SAR values. Moreover, by using our proposed defective ground structure (DGS) enabled design any 2×2 MIMO rim antenna can achieve up to 30%

Received 21 February 2022, Accepted 13 March 2022, Scheduled 24 March 2022

* Corresponding author: Muhammad Ali Jamshed (mohammadalijamshed@gmail.com).

[1] James Watt School of Engineering, University of Glasgow, UK. [2] Institute of Communication Systems (ICS), Home of 5G and 6G Innovation Centres, University of Surrey, UK.

reduction in the SAR in comparison to their baseline value. To the best of the authors' knowledge, this is the first work to investigate the SAR reduction capability by utilizing MIMO antennas implemented in the rim of a smartphone.

The rest of the paper is organized as follows. Section 2 of the paper explains the geometry and the working of the proposed antenna. In Section 3, the fabrication and simulation of our prototype antenna are discussed and measured results are compared. Moreover, Section 3 also studies the variation in the MIMO performance of the antenna when changing the levels of mutual coupling. Section 4 validates the reduction in the SAR as well as studies the effects of the LCD and hand on antenna efficiency when changing the level of coupling. Finally, we conclude the paper in Section 5.

2. ANTENNA GEOMETRY AND WORKING PRINCIPLE

Two resonant frequencies of 2.1 GHz and 4.3 GHz are achieved by the proposed antenna based on the points at which the rim is fed by two ports at the right and left side of the UT. These feeds are assisted by a DGS that manipulate the ground surface current as well as the characteristic modes and subsequently the SAR discussed in this section.

2.1. Geometry of the Proposed Antenna

Figure 1 illustrates the geometry of our proposed dual band 2×2 MIMO rim based antenna design. The chassis of the antenna is 132 mm $\times$ 74 mm, which is typical of any smartphone available in the market. A 0.8 mm thick single sided FR-4, having a permitivity of $\epsilon_r = 4.4$ is used as a substrate material. The 0.3 mm thick metal plates are used to cover the surroundings of chassis. Two 1 mm gaps are slit in the shorter edges to activate the higher resonance modes [10], whereas to control the amount of coupling between antenna elements, two 10 mm gaps are slit on the longer edges. Since most of the portion of the metallic rim is shorted to the ground plane, wider slits are then needed on the longer edges to separate the DGS and the rim. The dimensions of each element and the ground clearance are shown in Fig. 1. The two periodic DGSs are placed exactly at the centre of the two antenna elements to avoid the imbalance in the level of coupling between the two antenna elements and is controlled by using diodes (Infinenon, BAR50-02V are used). The two 100 pF RF signal blocking capacitors are employed at the edge of each DGS to avoid the mixing of AC and DC. Two identical diode pairs are sufficient to change the levels of coupling at 4.3 GHz. Whereas, the required length of the DGS needs to be comparatively smaller and it uses a single diode pair to achieve the variation in coupling at 2.1 GHz, due to the longer wavelength. Moreover, both antenna elements for each frequency are identical and symmetric.

2.2. Frequency Region Analysis

In this paper, we use the modal significance (MS) based on the theory of characteristic mode (TCM) [13], for gaining insights into the electromagnetic properties of our broken metal rim structure. At a given frequency, the $MS_n = 1$ indicates that an nth characteristic mode (CM) can potentially resonate [14]. We have performed CM on the broken metal rim frame to validate the dual band operation of our proposed antenna design by indicating the potential CMs at the desired operating frequencies. In Fig. 2(a), the current modes of a broken metal rim structure with a ground plane is found by using the integral equation solver in CST. The thickness of the whole structure is 0 mm and exhibits the properties of perfect electric conductor (PEC). For characteristic mode analysis (CMA) operation no feeding port is placed on the antenna structure. Fig. 2(b) shows that Mode 1 and Mode 2 resonates at 2.1 GHz having $MS = 1$, whereas in Fig. 2(c), Mode 1 can resonate at 4.3 GHz. There are many ways to excite these resonance modes, in this paper a folded dipole is used for this purpose.

2.3. Surface Current Distribution

We have performed a current distribution analysis to further explain how the dual band operation and DGS works. The simulated surface current plots at 2.1 GHz and 4.3 GHz, are shown in Fig. 3 and Fig. 4, respectively. Fig. 3(a) shows that the longer side of the shorter edge of metallic rim is responsible for exciting the resonance mode of 2.1 GHz, whereas the smaller side of the shorter edge of metallic rim

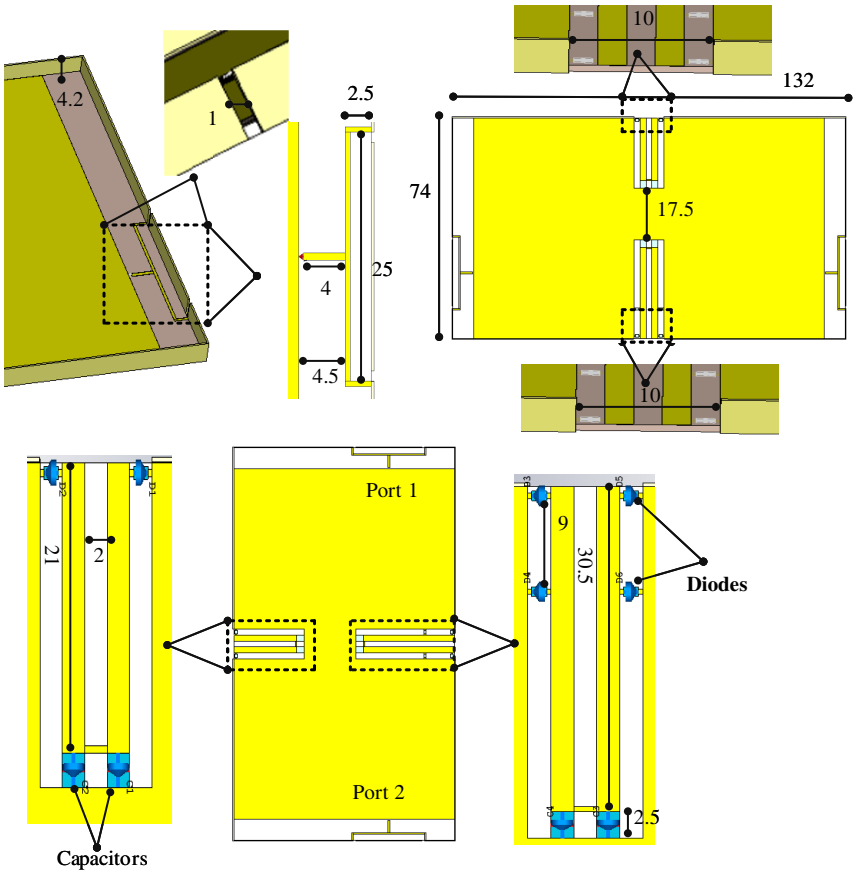

Figure 1. Geometry of the proposed dual band 2×2 MIMO-based rim antenna, with all the units in millimeters (mm) and the structure is displayed and explained using multiple views.

supports the resonance of 4.3 GHz in Fig. 3(b). Meanwhile, Fig. 3(a) shows that the current mainly concentrates on the left side of the folded dipole branch, and hence produces a $\lambda/4$ resonant mode, similar to a monopole structure. Fig. 3(b), illustrates that the current is near equally distributed on both arms of the folded dipole and results in a $\lambda/2$ resonant mode, similar to a dipole structure. Fig. 4, shows the variation in the surface current, when DGSs are either off or on by altering the level of DC voltage at the diodes. Figs. 4(a) and (c) show the variations of the surface current when altering the antenna coupling at 2.1 GHz. A noticeable change in the current levels can be seen either by activating or deactivating the DGS, which shows that the amount of antenna coupling can be effectively controlled using the DGS. A similar observation can be made for the DGS responsible for controlling the coupling levels at 4.3 GHz.

3. ANTENNA MEASUREMENTS

In order to validate our antenna design through experimental results, we have fabricated its mock-up prototype, as shown in Fig. 5. More precisely, two versions of it has been fabricated to avoid fabrication errors, i.e., one version mimicking the DGS ON configuration (see Fig. 5(a)), which uses passive connections to activate the DGS, and one version mimicking the DGS OFF configuration (see Fig. 5(b)). Fig. 6 depicts and compares the simulated and measured S-parameters for both configurations as a function of the frequency. Given the symmetry of our antenna structure, only the results of a single port are shown here. The simulated and measured S-parameter results are in good agreement and clearly show a change in the coupling levels by activating and deactivating the DGS. For instance, based on simulation data, the coupling level at 2.1 GHz is varied approximately between -11 and -14 dB, and at

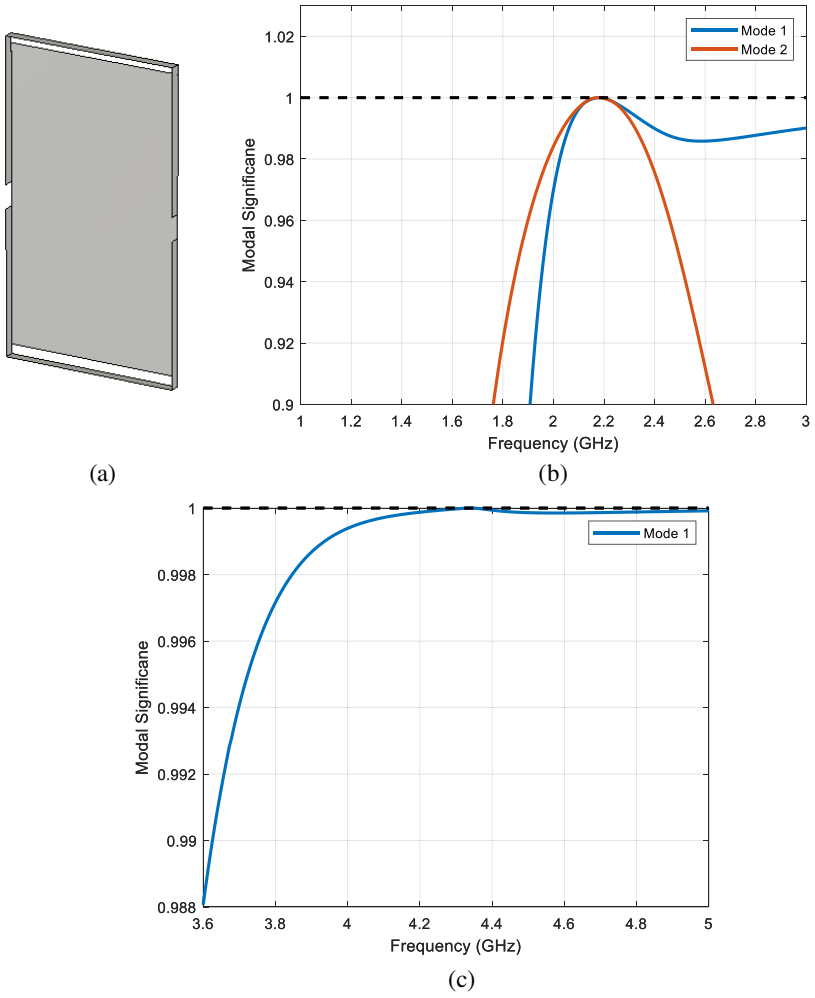

Figure 2. An illustration of the CMA analysis of the broken metallic rim. (a) Ground with broken metal rim model for CMA. (b) Modal significance at lower band. (c) Modal significance at higher band.

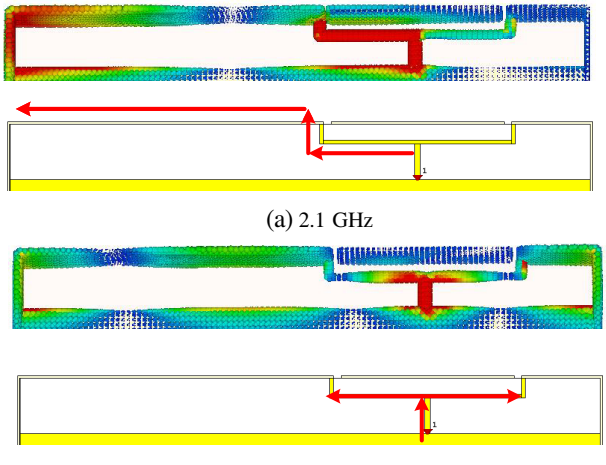

(a) 2.1 GHz

(b) 4.3 GHz

Figure 3. Simulated surface current plots at 2.1 GHz and 4.3 GHz.

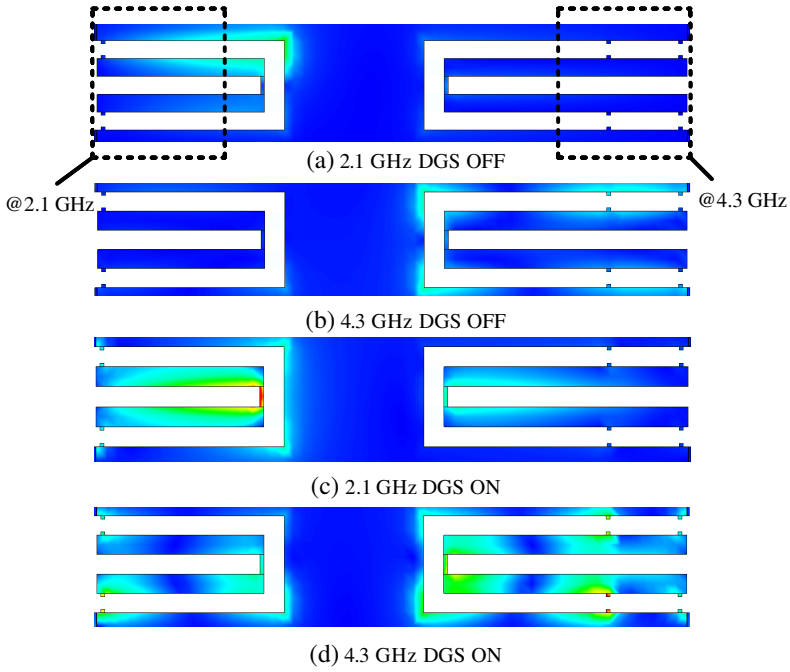

Figure 4. Simulated surface current plots at 2.1 GHz and 4.3 GHz for the DGS ON and OFF used cases.

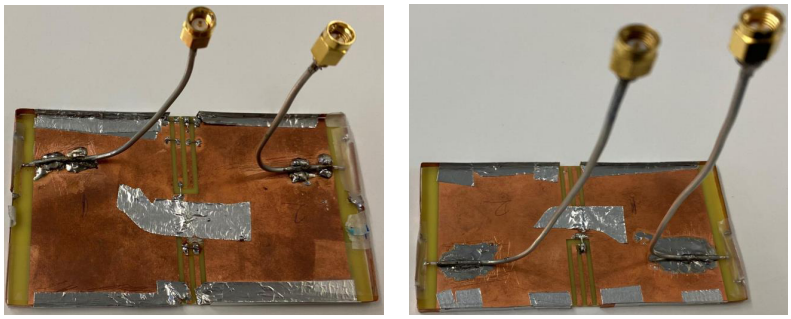

Figure 5. Prototype of (a) DGS ON configuration, (b) DGS OFF configuration of the proposed rim antenna design.

4.3 GHz is approximately between −13 and −18 dB, when the DGS is either activated or deactivated. In Fig. 7, the simulated and measured normalized radiation pattern for the four cases, i.e., at 2.1 GHz DGS ON and OFF, at 4.3 GHz DGS ON and OFF, are compared. A near omnidirectional radiation pattern is observed at the two frequencies for both DGS ON and OFF cases. These dipole like radiation pattern are suitable for communication in a practical environment. The radiation patterns are not affected by changing the level of antenna coupling, except a small variation is observed in measured radiation pattern at 2.1 GHz DGS OFF case, which is likely due to the inaccuracies in the measurement campaign and/or fabrication errors.

3.1. MIMO Performance

The mutual coupling has a significant role in determining the MIMO performance of an antenna design. It is well-known that any coupling level below −15 dB hardly impact the MIMO performance [15]. However, it is clear from Fig. 6 that the level of coupling of our antenna can be up to −11 dB, so it

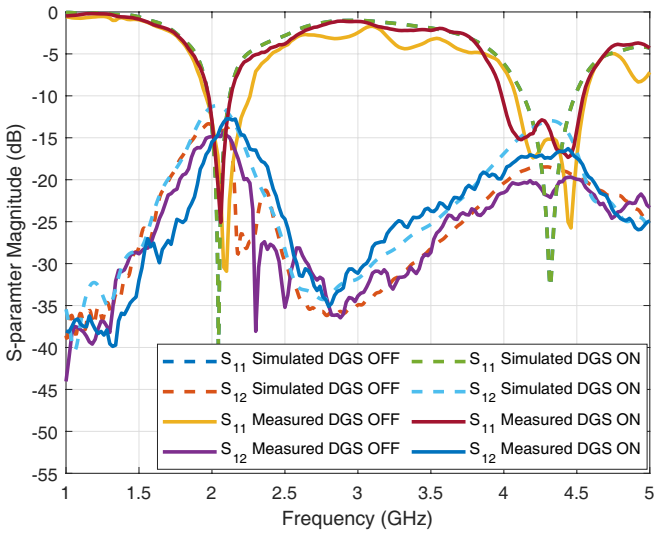

Figure 6. Comparison of the simulated vs measured S-parameters.

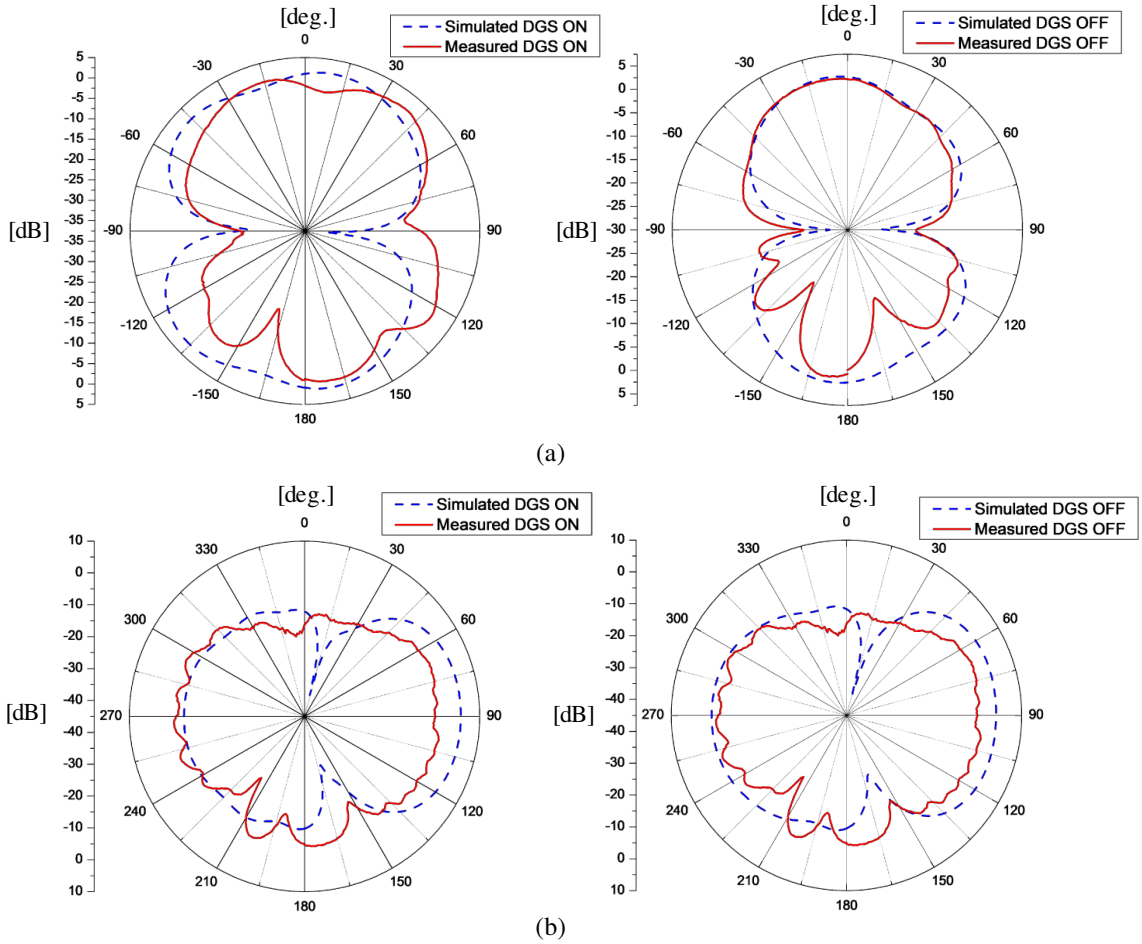

Figure 7. Comparison of simulated vs measured far-field radiation pattern, (a) 2.1 GHz in Azimuth, (b) 4.3 GHz in Elevation.

important to study its impact. The ECC has a direct impact on the spectral efficiency of the system [16], so along with the loss in capacity, it important to show its effect as well. The mathematical formulation for the capacity loss and the ECC in terms of S-parameter can be found in [16]. The measured values of ECC for DGS OFF case is 0.00017 at 2.1 GHz and 0.00084 at 4.3 GHz, whereas for DGS ON case it is 0.01 at 2.1 GHz and 0.002 at 4.3 GHz. The measured loss in capacity for DGS OFF case is 0.101 at 2.1 GHz and 0.109 at 4.3 GHz, whereas for DGS ON case it is 0.28 at 2.1 GHz and 0.19 at 4.3 GHz. It can be remarked that the ECC and the loss in capacity, calculated by using the measured S-parameter are below the required threshold, i.e., 0.4 bits/sec/Hz and 0.05, to operate in MIMO mode. Moreover, it is important to note that by increasing the level of antenna coupling the loss in capacity and the ECC increases, and the gap between the threshold and the calculated values decreases.

4. SAR AND EFFICIENCY ANALYSIS

An increase in mutual coupling can reduce SAR, when the UT comes in close contact to the human body. This has been validated by an in-depth SAR analysis and by placing the proposed antenna close to the human body in most common used positions. The three positions are illustrated in Fig. 8, i.e., placing the handset close to head, in front or in side pockets. The Gustav (a male heterogeneous biological replication of human body) voxel model is used for the analysis. The maximum averaged SAR for 10 g of body is calculated using IEEE/IEC 62704-1 method [17], the 23 dBm transmit power (uplink transmit power for LTE) is distributed equally between the two elements and both the elements are co-phased. Table 1 shows the variation in SAR values at both 2.1 and 4.3 GHz, and it can clearly be seen that the SAR is reduced when activating the DGS for each of the used cases. For instance at 2.1 GHz, when the UT is close to the head, the SAR is effectively reduced by 30%, whereas at 4.3 GHz the reduction in SAR is about 14%. This is due to the fact that the level of antenna coupling is higher for both frequencies when the DGS is activated, as shown in Fig. 6. Moreover, as shown in Fig. 4, the coupling between the antennas increases when the DGS is activated, which results in a decrease in the near field coupling from each antenna element towards the human body, and hence reduces SAR.

In Table 2, we have compared our work in terms of SAR with [10–12]. For a fair comparison, the antennas reported in [10–12] are reproduced and their SAR values are calculated using a similar setup (both elements are co-phased and power is equally split between them) used in this paper and only

Table 1. Variation in SAR values for DGS ON and OFF cases.

Resonance Frequencies	SAR 10 g (W/Kg)	Resonance Frequencies	SAR 10 g (W/Kg)	Resonance Frequencies	SAR 10 g (W/Kg)
DGS ON (Talk Position)		DGS ON (Front Pocket)		DGS ON (Side Pocket)	
@2.1 GHz	0.897	@2.1 GHz	0.133	@2.1 GHz	0.324
@4.3 GHz	0.973	@4.3 GHz	0.134	@4.3 GHz	0.201
DGS OFF (Talk Position)		DGS OFF (Front Pocket)		DGS OFF (Side Pocket)	
@2.1 GHz	1.285	@2.1 GHz	0.188	@2.1 GHz	0.410
@4.3 GHz	1.141	@4.3 GHz	0.139	@4.3 GHz	0.241

Table 2. Comparison with State-of-the-art.

Antennas	SAR 10 g (W/kg)
[10]	1.718
[11]	1.446
[12]	1.193
Proposed DGS ON	0.897

for the position when the handset is close to the head (cheek position [18]) with handgrip. The results reported in Table 2 shows that our proposed design can reduce the SAR by a fair amount.

A detailed analysis has been carried out to study the variation in the total antenna efficiency when activating or not the DGS in free space, and taking into account the LCD and human hand. Fig. 9 shows the simulation setup for the total antenna efficiency analysis. The CTIA posable hand model with a spacer having $\epsilon_r = 1$ is used to mimic the hand effects. The results for these variations are recorded in Table 3, and it shows that an acceptable antenna efficiency is still maintained even for the worst case scenario, where the antenna equipped with a LCD, gripped using a human hand, and posses a high coupling level. For instance, for port 1, when operating at 2.1 GHz in free space a 2% variation in total antenna efficiency is observed between the DGS ON and OFF case.

Table 3. Variation in the total antenna efficiency.

Antenna Ports	Free Space (dB)	LCD (dB)	Hand (dB)	LCD + Hand (dB)
DGS ON				
Port 1 @2.1 GHz	−0.95	−1.66	−2.02	−2.52
Port 1 @4.3 GHz	−0.85	−1.32	−1.75	−2.16
Port 2 @2.1 GHz	−0.95	−1.66	−2.21	−2.13
Port 2 @4.3 GHz	−0.85	−1.32	−2.75	−2.79
DGS OFF				
Port 1 @2.1 GHz	−0.78	−1.47	−2.04	−2.58
Port 1 @4.3 GHz	−0.39	−0.85	−1.34	−1.72
Port 2 @2.1 GHz	−0.78	−1.47	−2.34	−2.25
Port 2 @4.3 GHz	−0.39	−0.85	−2.47	−2.43

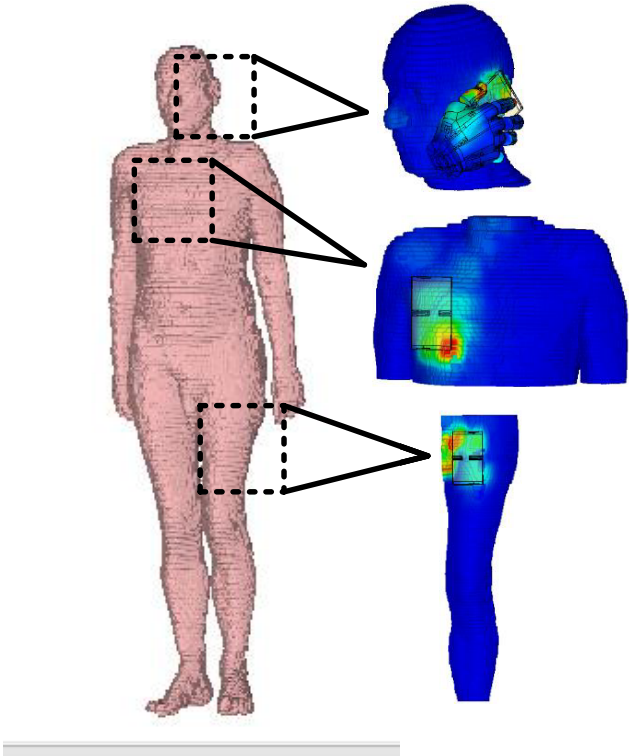

Figure 8. An illustration of a voxel model to study the effect of SAR on changing the antenna coupling.

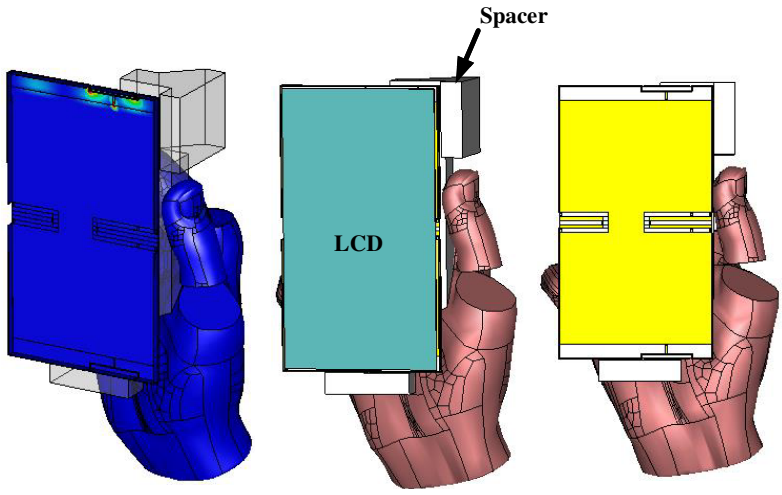

Figure 9. An illustration of the effect of hand and LCD on the proposed rim antenna design.

5. CONCLUSION

In this paper, the mutual coupling is used to alter the level of SAR. A dual band 2 element MIMO-based rim antenna design is proposed, which uses a periodic DGS to effectively increase the level of mutual coupling, when the UT comes in close contact. The working of the proposed antenna is validated using CMA and the current distributions. The proposed antenna is fabricated and the simulated and measured results are compared. The measured and simulated data shows an acceptable MIMO performance, and the SAR analysis supports the proposed design. The impact of hand and LCD on the performance of the proposed antenna is studied and it shows an acceptable variation in total antenna efficiency. Conclusively, the proposed antenna helps to set up a new domain to design the context-aware UTs.

ACKNOWLEDGMENT

This work has been funded by EPSRC under the grant agreement "EP/P005853/1: Electromagnetic field exposure reduction/avoidance for the next generations of wireless communication systems". We would also like to acknowledge the support of the University of Surrey, ICS (http://www.surrey.ac.uk/5gic) members for this work.

REFERENCES

1. Li, W., W. Lin, and G. Yang, "A compact MIMO antenna system design with low correlation from 1710 MHz to 2690 MHz," *Progress In Electromagnetics Research*, Vol. 144, 59–65, 2014.
2. Ren, A., Y. Liu, et al., "A compact building block with two shared-aperture antennas for eight-antenna mimo array in metal-rimmed smartphone," *IEEE Transactions on Antennas and Propagation*, Vol. 67, No. 10, 6430–6438, 2019.
3. Sun, L., Y. Li, Z. Zhang, and Z. Feng, "Wideband 5g mimo antenna with integrated orthogonalmode dual-antenna pairs for metal-rimmed smartphones," *IEEE Transactions on Antennas and Propagation*, Vol. 68, No. 4, 2494–2503, 2019.
4. Ban, Y.-L., C. Li, G. Wu, K.-L. Wong, et al., "4g/5g multiple antennas for future multi-mode smartphone applications," *IEEE Access*, Vol. 4, 2981–2988, 2016.
5. Wong, K.-L., C.-Y. Tsai, J.-Y. Lu, D.-M. Chian, and W.-Y. Li, "Compact eight mimo antennas for 5g smartphones and their mimo capacity verification," *2016 URSI Asia-Pacific Radio Science Conference (URSI AP-RASC)*, 1054–1056, IEEE, 2016.

6. Jamshed, M. A., F. Heliot, and T. W. Brown, "A survey on electromagnetic risk assessment and evaluation mechanism for future wireless communication systems," *IEEE Journal of Electromagnetics, RF and Microwaves in Medicine and Biology*, Vol. 4, No. 1, 24–36, 2019.
7. Kitra, M. I., C. J. Panagamuwa, P. McEvoy, J. C. Vardaxoglou, and J. R. James, "Low sar ferrite handset antenna design," *IEEE Transactions on Antennas and Propagation*, Vol. 55, 1155–1164, Apr. 2007.
8. Wang, J., O. Fujiwara, and T. Takagi, "Effects of ferrite sheet attachment to portable telephone in reducing electromagnetic absorption in human head," *IEEE International Symposium on Electromagnetic Compatability*, Vol. 2, 822–825, Aug. 1999.
9. Gómez-Villanueva, R., H. Jardón-Aguilar, and R. L. y Miranda, "State of the art methods for low sar antenna implementation," *Proceedings of the Fourth European Conference on Antennas and Propagation*, 1–4, Apr. 2010.
10. Stanley, M., Y. Huang, H. Wang, H. Zhou, Z. Tian, and Q. Xu, "A novel reconfigurable metal rim integrated open slot antenna for octa-band smartphone applications," *IEEE Transactions on Antennas and Propagation*, Vol. 65, No. 7, 3352–3363, 2017.
11. Ban, Y.-L., Y.-F. Qiang, G. Wu, H. Wang, and K.-L. Wong, "Reconfigurable narrow-frame antenna for lte/wwan metal-rimmed smartphone applications," *IET Microwaves, Antennas & Propagation*, Vol. 10, No. 10, 1092–1100, 2016.
12. Zhang, L.-W., Y.-L. Ban, J. Guo, Z.-F. Yu, et al., "Parallel dual-loop antenna for WWAN/LTE metalrimmed smartphone," *IEEE Transactions on Antennas and Propagation*, Vol. 66, No. 3, 1217–1226, 2018.
13. Garbacz, R. and R. Turpin, "A generalized expansion for radiated and scattered fields," *IEEE Transactions on Antennas and Propagation*, Vol. 19, No. 3, 348–358, 1971.
14. Chen, Y. and C.-F. Wang, *Characteristic Modes: Theory and Applications in Antenna Engineering*, John Wiley & Sons, 2015.
15. Chen, X., S. Zhang, and Q. Li, "A review of mutual coupling in MIMO systems," *IEEE Access*, Vol. 6, 24706–24719, 2018.
16. Chae, S. H., S.-K. Oh, and S.-O. Park, "Analysis of mutual coupling, correlations, and TARC in WiBro MIMO array antenna," *IEEE Antennas and Wireless Propagation Letters*, Vol. 6, 122–125, 2007.
17. "IEC/IEEE International Standard — Determining the peak spatial-average specific absorption rate (SAR) in the human body from wireless communications devices, 30 MHz to 6 GHz — Part 1: General requirements for using the finite-difference time-domain (FDTD) method for SAR calculations," *IEC/IEEE 62704-1:2017*, 1–86, Oct. 2017.
18. "IEEE recommended practice for determining the peak spatial-average specific absorption rate (SAR) in the human head from wireless communications devices: Measurement techniques," *IEEE Std 1528-2013 (Revision of IEEE Std 1528-2003)*, 1–246, Sep. 2013.